Gate-controlled supercurrent in ballistic InSb nanoflag Josephson junctions $_{EP}$

Sedighe Salimian, Matteo Carrega, Isha Verma, et al.

COLLECTIONS

EP This paper was selected as an Editor's Pick

View Online   Export Citation   CrossMark

ARTICLES YOU MAY BE INTERESTED IN

Multiqubit entanglement and quantum phase gates with epsilon-near-zero plasmonic waveguides
Applied Physics Letters **119**, 211104 (2021); https://doi.org/10.1063/5.0071797

WSe_2/Pd Schottky diode combining van der Waals integrated and evaporated metal contacts
Applied Physics Letters **119**, 213102 (2021); https://doi.org/10.1063/5.0064550

Photoluminescence, stimulated and laser emission in $CuInSe_2$ crystals
Applied Physics Letters **119**, 212103 (2021); https://doi.org/10.1063/5.0060076

Gate-controlled supercurrent in ballistic InSb nanoflag Josephson junctions ᴱᴾ

Sedighe Salimian,[1] (iD) Matteo Carrega,[2] Isha Verma,[1] Valentina Zannier,[1] (iD) Michał P. Nowak,[3] (iD) Fabio Beltram,[1] Lucia Sorba,[1] and Stefan Heun[1,a)] (iD)

AFFILIATIONS

[1] NEST, Istituto Nanoscienze-CNR and Scuola Normale Superiore, Piazza San Silvestro 12, 56127 Pisa, Italy
[2] CNR-SPIN, Via Dodecaneso 33, 16146 Genova, Italy
[3] AGH University of Science and Technology, Academic Centre for Materials and Nanotechnology, al. A. Mickiewicza 30, 30-059 Krakow, Poland

[a)] Author to whom correspondence should be addressed: stefan.heun@nano.cnr.it

ABSTRACT

High-quality III–V narrow bandgap semiconductor materials with strong spin–orbit coupling and large Landé g-factor provide a promising platform for next-generation applications in the field of high-speed electronics, spintronics, and quantum computing. Indium antimonide (InSb) offers a narrow bandgap, high carrier mobility, and small effective mass and, thus, is very appealing in this context. In fact, this material has attracted tremendous attention in recent years for the implementation of topological superconducting states supporting Majorana zero modes. However, high-quality heteroepitaxial two-dimensional (2D) InSb layers are very difficult to realize owing to the large lattice mismatch with all commonly available semiconductor substrates. An alternative pathway is the growth of free-standing single-crystalline 2D InSb nanostructures, the so-called nanoflags. Here, we demonstrate fabrication of ballistic Josephson-junction devices based on InSb nanoflags with Ti/Nb contacts that show a gate-tunable proximity-induced supercurrent up to 50 nA at 250 mK and a sizable excess current. The devices show clear signatures of subharmonic gap structures, indicating phase-coherent transport in the junction and a high transparency of the interfaces. This places InSb nanoflags in the spotlight as a versatile and convenient 2D platform for advanced quantum technologies.

Today, great interest revolves around the possibility to create and manipulate new states of matter with topological properties. This stems mostly from the intrinsic robustness of topological states against local perturbation and the ensuing relevance for quantum computing architectures.[1,2] Hybrid superconductor/semiconductor heterostructures represent a promising platform in which topological properties can emerge.[3–6]

In this context, indium antimonide (InSb) has attracted much attention recently. InSb has a narrow bandgap ($\sim$0.23 eV).[6–8] It also has a very high bulk electron mobility [7.7×10^4 cm^2/(V s)][9,10] and a small effective mass ($m^* = 0.018\,m_e$),[8,9,11–14] which are both important requirements for high-speed and low-power electronic devices.[10,15] Finally, it also exhibits a strong spin–orbit interaction and a large Landé g-factor ($|g^*| \sim 50$[9,14]), and thus, it is useful for spintronics applications[8,15] and for the creation of hybrid structures hosting topological states like Majorana zero-modes. Indeed, the first signatures compatible with Majorana bound states were reported in

InSb nanowires coupled to a superconductor,[3,16] which has triggered strong efforts to improve the quality of hybrid systems based on InSb nanowires.[17–24]

Aside from one-dimensional nanowires, two-dimensional (2D) InSb structures also attract great attention, owing to their inherent design flexibility.[6,8,14] Indeed, InSb 2D electron gases[12] and the related ternary compound InSbAs[6] have recently been proposed as a platform for topological superconductivity,[25] and ballistic superconductivity was demonstrated in InSb quantum wells.[12] However, the growth of high-quality heteroepitaxial 2D InSb layers is still a challenge owing to their large lattice mismatch with common semiconductor substrates. In addition, such quantum wells are reported to suffer from instabilities due to the Si dopants.[14] A possible strategy to circumvent these problems consists in growing free-standing 2D InSb nanostructures on nanowire stems, because nanowires yield efficient relaxation of elastic strain along the nanowire sidewalls, when lattice-mismatched semiconductor systems are integrated. To emphasize their free-

standing 2D shape, such nanostructures are often referred to as nano-sails, nanosheets, nanoflakes, or nanoflags. However, until today, only a few studies were reported on the growth and the electrical transport properties of such InSb nanoflags (NFs).[7,9,13,19,26–30]

InSb NFs were first reported in 2016 by de la Mata et al.[9] their growth being based on molecular beam epitaxy (MBE). There, the authors attributed the 2D geometry of the NFs to a single twinning event in the otherwise pure zinc blende structure of the InSb sample, and four-terminal electrical measurements revealed an electron mobility greater than $12\,000\ \mathrm{cm^2/(V\,s)}$. Pan et al. used Ag-assisted MBE to grow free-standing 2D single-crystalline InSb NFs.[26] Hall-bar devices were then fabricated that showed ambipolar behavior and an electron mobility of $18\,000\ \mathrm{cm^2/(V\,s)}$. The same group also demonstrated functional InSb NF Josephson junctions (JJs) with Al and Nb contacts.[27] Furthermore, in the devices with Nb contacts, the authors reported evidence of the coexistence of the quantum Hall effect and proximity-induced superconductivity in the InSb NFs.[28] Quantum transport and quantum-dot geometries in such nanostructures were also demonstrated very recently.[7,31–33] Gazibegovich et al. combined selective-area growth with the vapor-liquid-solid mechanism in metal organic vapor phase epitaxy, leading to the formation of InSb NFs thanks to the development of a twin-plane boundary.[19,34] The same group reported evidence for crossed Andreev reflections in JJs made from such flakes.[13]

Also our group demonstrated the growth of single-crystal, free-standing InSb NFs, initially on InAs nanowires, using a directional growth technique based on chemical beam epitaxy (CBE).[29] The NF size was limited by the flexibility of the InAs nanowires, which led to a bending of the stem and the resulting loss of the orientation for the asymmetric 2D growth. In order to overcome this issue, we recently optimized the growth of InSb NFs.[30] In particular, the InSb NFs were grown on sturdy tapered InP nanowires, which did not bend and allowed to grow larger NFs with the same directional-growth approach. This strategy allowed us to obtain InSb NFs of (2.8 ± 0.2) μm length, (470 ± 80) nm width, and (105 ± 20) nm thickness.[30]

The resulting NFs are large enough to fabricate Hall bars with length-to-width ratios enabling precise electrical characterization. An electron mobility of $29\,500\ \mathrm{cm^2/(V\,s)}$ was measured at a carrier concentration $n = 8.5 \times 10^{11}\ \mathrm{cm^{-2}}$ at 4.2 K.[30] The electron elastic mean free path ℓ_e reached values of 500 nm, which favorably compares with the literature.[9,13,34]

Here, we report on the fabrication and characterization of JJ devices based on these InSb NFs and provide evidence of ballistic superconductivity. We employ Ti/Nb contacts in InSb JJ devices and show both gate-tunable proximity-induced supercurrent at 250 mK and sizable excess current. The devices also show clear signatures of subharmonic gap structures, indicating phase-coherent transport in the junction and highly transparent interfaces. Our results indicate InSb NF as a promising platform for the study of topological superconductivity.

The upper left inset of Fig. 1 shows a SEM image of the device investigated in this work (for consistent results from other devices, see the supplementary material). In brief, a 100 nm-thick InSb NF was transferred mechanically on a SiO_2/Si substrate and contacted with 10/150 nm Ti/Nb. (More details on device fabrication are provided in the supplementary material.) The interelectrode spacing between the two superconductors, i.e., the length of the normal (N) region, is $L = 200$ nm, while its width is $W = 700$ nm. Standard transport
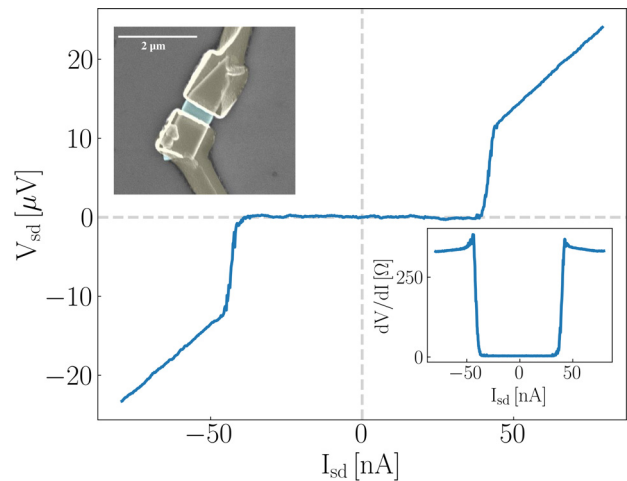

FIG. 1. DC voltage drop V_{sd} as a function of the bias current I_{sd}. A supercurrent of $\sim$50 nA is observed. The lower right inset shows the differential resistance dV/dI measured simultaneously by the lock-in technique. $V_{bg} = 30$ V, $T = 250$ mK. $B = 6$ mT applied to compensate for the residual magnetization of the cryostat. The upper left inset shows an SEM image of the device structure. Scale bar 2 μm.

characterization yields a mean-free path of $\ell_e \sim 500$ nm[30] for the N region, greater than the junction length L. These numbers place the device in the ballistic regime.

The critical temperature of the superconducting leads was determined to be $T_c = 8.44$ K, from which the bulk gap can be computed using the theory by Bardeen, Cooper, and Schrieffer (BCS):[35] $\Delta = 1.76 k_B T_c = 1.28$ meV, consistent with values of Nb superconducting contacts previously reported in the literature.[28,36–41] The induced superconducting coherence length[13,27,42,43] is $\xi_s = \hbar v_F / \Delta$, with v_F being the Fermi velocity in the N region ($v_F = 1.5 \times 10^6$ m/s) and Δ being the gap in the superconductor. Here, $\xi_s \sim 750$ nm $> L$, so the device is in the short junction regime. Equivalently, the Thouless energy[42,44] $E_{Th} = \hbar v_F / L = 4.9$ meV $> \Delta$.

Figure 1 shows typical voltage–current ($V - I$) characteristics obtained at $T = 250$ mK and $V_{bg} = 30$ V. The device displays well-developed dissipationless transport, thus demonstrating proximity-induced superconductivity in the InSb NF. As the bias current exceeds the critical value of $\sim$50 nA, a sudden jump in the measured voltage to a dissipative quasiparticle branch is observed, indicating that the JJ switches from the superconducting to the normal state with a resistance of $\sim$330 Ω. Current sweeps in opposite directions show negligible hysteresis, i.e., switching and retrapping current are the same, so that in the following, we shall use the switching current and critical current as synonyms. Consistently, the switching current is larger than the intrinsic thermal current noise δI_{th} of the junction[27,45] $\delta I_{th} = 2e k_B T / \hbar$; here, $\delta I_{th} = 10.5$ nA. The lower right inset to Fig. 1 shows the differential resistance dV/dI measured using a lock-in amplifier together with the $V - I$ curve. Data clearly show that the differential resistance is zero in the supercurrent branch of the device. Zhi et al. report a supercurrent of 20 nA at 10 mK in Nb/InSb nanoflag SNS junctions.[27] We attribute the improved numbers reported here mainly to a higher mobility of the nanoflags and progress in device fabrication.

Superconducting quantum interference was observed in the dependence of the supercurrent on a magnetic field applied
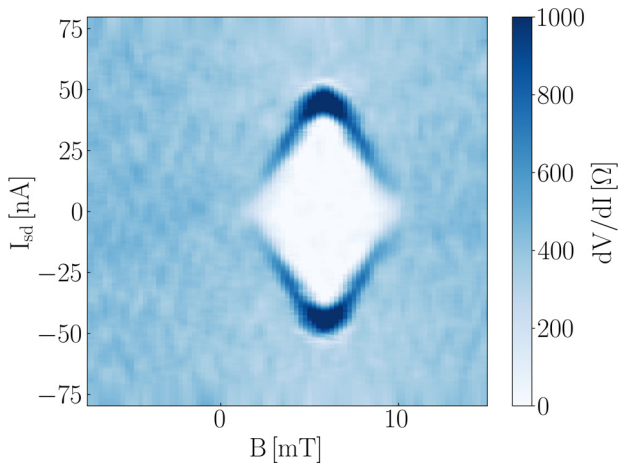
FIG. 2. 2D colormap of differential resistance dV/dI, obtained by numerical derivation of measured DC $V - I$ curves, plotted vs current bias I_{sd} and magnetic field B, measured at $V_{bg} = 40$ V and $T = 250$ mK.

perpendicularly to the sample plane (Fig. 2). Supercurrent maximum is obtained for $B_0 = 6$ mT instead of the expected maximum at zero B field. This small offset can be attributed to a residual magnetization in the cryostat. Applying higher or lower magnetic fields, the supercurrent symmetrically decreases, until for $|B - B_0| > 5.2$ mT it is suppressed. The modulation of the critical current by quantum interference is one of the hallmarks of the Josephson effect. The shape of the curve resembles a Fraunhofer pattern with only the central lobe, i.e., without side-lobes. We have verified that in a magnetic field range of $B \leq 50$ mT, no side-lobes appear. de Vries et al. have studied similar InSb NF JJs and report an even-odd Fraunhofer pattern.[13] Thus, the intensity of the first side-lobes might be anomalously small, which precludes their observation in our experiment. On the other hand, such anomalous magnetic interference patterns, with a monotonous decay, were reported previously in similar geometries[36,37,46,47] and were attributed to geometric factors.[36,46,48–53] In addition, the magnetic flux through the junction is $\Phi = B \cdot A$, with A the junction area, $A = W(L + 2\lambda_L)$.[54] Here, λ_L is the London penetration depth of Nb. Thus, the smaller the channel width W, the higher the value of B required to reach $\Phi = \Phi_0$. According to Rohlfing et al.,[36] larger values of B more strongly suppress $I_c(B)$ via a dramatic reduction of the

amplitude of Andreev reflections. Future measurements on devices with larger W/L ratio might help us to clarify whether the missing lobes in Fig. 2 are due to geometric factors.

InSb NFs are n-type semiconductors, and the carrier concentration in the NF can be tuned by an applied gate voltage.[30] Figure 3(a) shows that the global gate modulation can also be employed to control the magnitude of the supercurrent maximum. The figure shows the differential resistance dV/dI of the device as a function of the current bias I_{sd} and the back gate voltage V_{bg}. The central white region represents the zero-resistance supercurrent branch. In a range of gate voltages from 20 to 50 V, the supercurrent is approximately constant at ~ 50 nA. Decreasing the gate voltage below 20 V, the supercurrent decreases, until it disappears for ~ 5 V. This demonstrates the gate voltage control of the supercurrent magnitude and that the device implements a Josephson field effect transistor (JoFET).[55–59] The corresponding $V - I$ curves as a function of the back gate voltage are shown in Fig. 3(b) as line plots. While the $V - I$ curve for $V_{bg} = 10$ V still shows a zero slope at the origin, already for $V_{bg} = 7$ V the $V - I$ curve is essentially linear with Ohmic behavior. The gate voltage dependence of the switching current is shown in Fig. 3(b) as red line and confirms that below $V_{bg} = 20$ V the switching current decreases. The normal resistance (the slope of the $V - I$ curves in the normal branch) displays an opposite behavior: below $V_{bg} = 20$ V, it increases significantly from ~ 330 Ω to above 10 kΩ. The product of the switching current and normal resistance, $I_{sw} \cdot R_n$, is approximately constant at 15 μV in a wide range from $V_{bg} = 10$ V to 50 V (see Fig. S1 in the supplementary material), while it drops to zero when the switching current becomes zero. Similar results were reported by Zhi et al.[27]

Next, we characterize the dissipative regime. Figure 4(a) shows subharmonic gap structures in the differential conductance that can be attributed to multiple Andreev reflections (MARs). The peak present at $V_{sd} = 0$ V corresponds to the superconductive state. On the other hand, above $V_{sd} \sim \pm 0.8$ mV, the differential conductance becomes constant and is equal to the inverse of the normal resistance, R_n^{-1}. Between these two extrema, the differential conductance dI/dV displays characteristic singularities (minima and maxima), which represent the subharmonic gap structures.[60–63] Their presence is a signature of the high transparency of the interfaces between S and N regions. The positions of these MAR singularities follow the equation $eV_n = 2\Delta^*/n$ with $n = 1, 2, 3, \ldots$ and Δ^* being the induced gap in the N region. Most commonly, the position of the maxima in the differential conductance has been analyzed,[6,12,13,18,27,28,36,41,64,65] but recently it
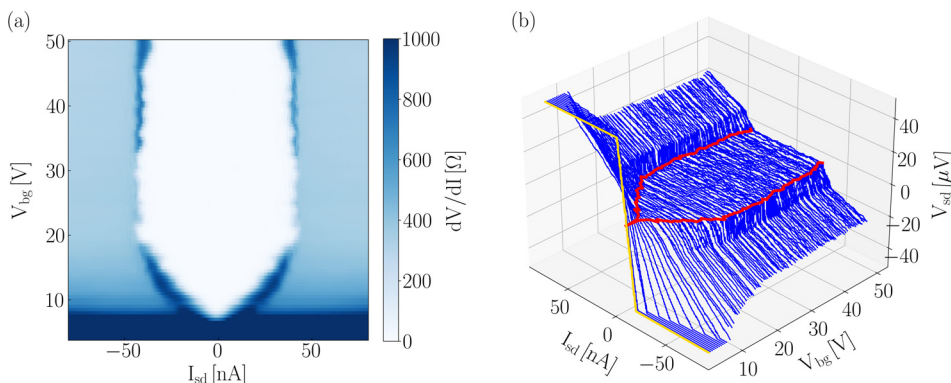

FIG. 3. (a) Color-scale plot of differential resistance dV/dI, measured by the lock-in technique, as a function of the current bias I_{sd} and back gate voltage V_{bg}. (b) 3D plot shows the trend of simultaneously measured DC $V - I$ curves at different back gate voltages. The first curve (at lowest back gate voltage) is highlighted in yellow. Red lines indicate the transition between the superconductive and the dissipative regime. The supercurrent increases with increasing the back gate voltage above pinch off. $T = 250$ mK. $B = 6$ mT applied to compensate for the residual magnetization of the cryostat.
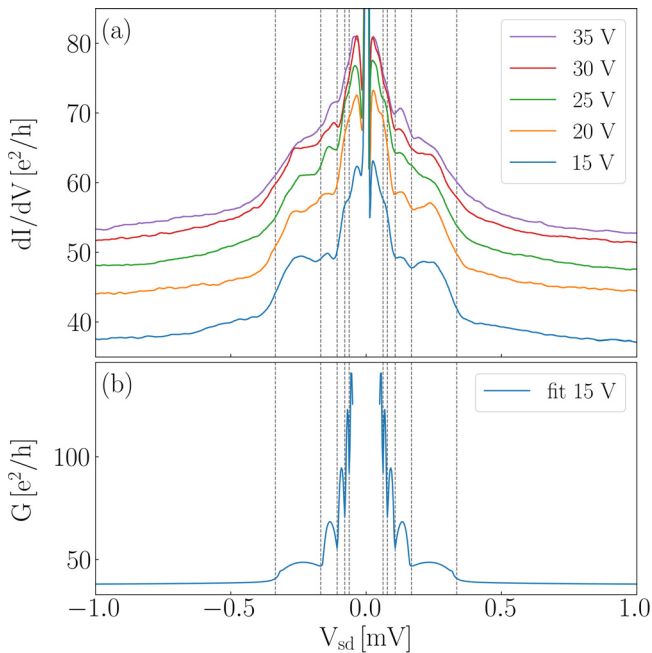
FIG. 4. (a) Differential conductance dI/dV, measured by the lock-in technique, as a function of the source-drain voltage V_{sd} for several back gate voltages V_{bg}, as indicated in the legend. The dashed lines indicate minima in differential conductance caused by multiple Andreev reflections ($n = \pm1$ to $n = \pm5$). $T = 250$ mK. $B = 6$ mT applied to compensate for the residual magnetization of the cryostat. (b) Conductance line trace obtained from a coherent scattering model vs source-drain voltage V_{sd}. The theoretical fit of the data for $V_{bg} = 15$ V yields a transmission $Tr = 0.94$ and a value of the induced gap of $\Delta^* = 160$ μeV.

FIG. 5. $I - V$ characteristics measured in DC. The linear fit (dashed line) of the $I - V$ curve for $V_{sd} > 2\Delta^*/e$ gives the excess current I_e as the intercept at zero bias voltage. The inset displays the excess current in a smaller bias voltage range. $T = 250$ mK and $V_{bg} = 40$ V. $B = 6$ mT applied to compensate for the residual magnetization of the cryostat.

was pointed out that for highly transparent junctions, the MAR resonances appear as minima in the differential conductance.[66]

In order to estimate the junction transparency and the induced gap, we used a simple scattering model that assumes fully coherent transport across a multimode JJ (see Ref. 67 and the supplementary material) and that has been applied to reproduce MAR traces of nanowire junctions.[68] Thus, the experimental curves were compared to optimized theoretical MAR conductance traces. One example is shown in Fig. 4(b). The best agreement between the experiment and theory is obtained for a junction model with 40 modes of transparency $Tr = 0.94$ and an induced gap of $\Delta^* = 160$ μeV.[69] The dashed vertical lines in Fig. 4 highlight the series from $n = \pm1$ to $n = \pm5$, showing an excellent agreement with the predicted behavior for the minima in differential conductance in a highly transparent junction.[66] Results of the analysis for the other back gate voltages are very similar. Consistently, while the transparency of the modes and the induced gap do not change with back gate voltage, the number of modes does: from less than 30 at $V_{bg} = 10$ V to more than 50 at $V_{bg} = 30$ V. The obtained value of the induced gap, $\Delta^* = 160$ μeV, is smaller than the value extracted from the measurement of the critical temperature. We note that similar values for the induced gap Δ^* have been reported for InSb nanowires proximitized by Nb[64] and by NbTiN.[16]

Aside from that differential conductance data, we recorded also DC traces ($I - V$ curves). Figure 5 shows a representative example obtained with $V_{bg} = 40$ V. From a linear fit of the part of the curve at
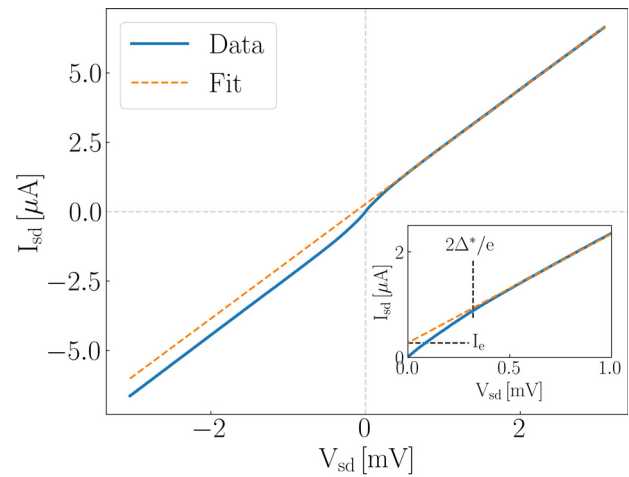
high bias, with $|V_{sd}| \geq 2\Delta^*$, where Andreev reflections are completely suppressed, we obtain an excess current of $I_e = 265\pm12$ nA and a normal resistance of $R_n = 481\pm3$ Ω. We add that the results do not change significantly if we consider only the voltage range $|V_{sd}| \geq 2$ meV. These numbers result in a product $I_e \cdot R_n = 127\pm7$ μV, an important figure of merit for weak links.[70] From $V_{bg} = 40$ to 20 V, the excess current is almost constant, while it decreases for smaller back gate values, to $\sim$50 nA at $V_{bg} = 5$ V. The normal resistance displays the opposite behavior: below $V_{bg} = 20$ V, it increases significantly to about 3.1 kΩ at $V_{bg} = 5$ V. As shown in the supplementary material, the product of the excess current and normal resistance, $I_e \cdot R_n$, remains approximately constant at 137 ± 19 μV over the whole range of back gate voltages explored, i.e., from $V_{bg} = 5$ V to 40 V.

We should like to analyze the superconducting-gap values as obtained from the critical temperature of the superconductor and the observed multiple Andreev-reflection features. The measured critical temperature $T_c = 8.44$ K is close to the reported value for bulk Nb, and the resulting value of the gap $\Delta = 1.28$ meV is in good agreement with values reported for JJs with Nb contacts.[28,36–41,65] Thus, we attribute the observed critical temperature to a switching of the Nb film from the superconducting state to the normal state.

On the other hand, several groups reported gap values extracted from an analysis of MAR features that were smaller than the BCS-like gap of the superconducting leads.[12,24,64] Kjaergaard et al. investigated multiple Andreev reflections in an InAs quantum-well heterostructure with epitaxial Al.[66] From an analysis of the MAR features, authors obtained a gap value smaller than the BCS-like gap Δ of Al and showed that this is due to an induced gap $\Delta^* < \Delta$ in the quantum well covered by Al. Andreev reflections of particles in the uncovered region occur at the (vertical) effective interface to the covered region with gap Δ^* in the quantum well. Since these reflections occur within the InSb crystal, the transparency of the process is high (here, $Tr = 0.94$).

Another relevant effect is the proximity-effect transfer from Nb into InSb via the thin Ti film. Drachmann *et al.* studied the proximity-effect transfer from a NbTi film into an InAs quantum well via a thin epitaxial Al layer.[71] They found that the induced gap Δ^* was increased by the NbTi film compared to samples with just the Al film, but it was still smaller than the BCS-like gap of NbTi. This implies that the proximity effect transfer can be weakened by an intermediate superconducting layer with smaller T_c. We recall that the reported T_c value for bulk Ti is ~ 0.5 K,[72,73] i.e., much smaller than the T_c of Nb. The combination of both effects is likely able to explain the observed value of the induced gap in our experiments.

The transparency of the (horizontal) interfaces between the superconducting electrodes and InSb can be estimated using the theory of Aminov *et al.*,[74] which measures the transparency via the dimensionless parameter γ_B ($\gamma_B = 0$ for perfectly transparent interfaces, larger γ_B for larger barriers). Using the BCS gap of Nb, we obtain $\gamma_B = 12.5$. Considering that the presence of the Ti film will slightly reduce the gap by an (unknown) amount, $\gamma_B \approx 10$. This indicates a small transparency of the interface, consistent with the fact that the induced gap is much smaller than the BCS gap of Nb. On the other hand, Kjaergaard *et al.*[66] and Baumgartner *et al.*[75] report $\gamma_B \sim 1$, consistent with their use of epitaxial Al/InAs heterostructures, which are known to have highly transparent interfaces.

Theory predicts for JJ at $T = 0$ that the product $I_c \cdot R_n$ is constant proportional to the gap, $I_c \cdot R_n = \alpha \Delta^*/e$, with the prefactor α being constant of order unity.[45,76–80] Here, $I_c \cdot R_n = 15$ μV is only about 10% of $\Delta^*/e = 160$ μV. Such a reduction is frequently observed in experiment[18,27,81] and has been attributed to a premature switching of the junction due to thermal activation.[76,82] On the other hand, excess current is due to Andreev reflections and, thus, depends primarily on the transparency of the (vertical) interface between the covered and uncovered parts of the semiconductor,[80] which is high. Consequently, a large product $I_e R_n \approx \Delta^*/e$ is observed, close to the theoretical value of 8/3 Δ^*/e for ballistic junctions.[63,80]

In summary, we have fabricated JJ devices with InSb NFs as the normal region and Ti/Nb as superconducting contacts. The high electron mobility and large mean free path of the InSb NFs yielded ballistic transport across the normal region of the junction. We showed Josephson coupling between the superconductor and semiconductor, as demonstrated by the zero-resistance supercurrent of ~ 50 nA and the observation of MARs. Analysis of the MAR traces indicates a very high transparency of the interfaces. We also observe a sizable excess current. Our results show that free-standing 2D InSb NFs on InP stems, thanks to their defect-free zinc blende crystal structure,[30] are a suitable material platform for fabrication of quantum devices. Considering also their strong spin–orbit interaction and their large Landé g-factor, we envision the use of these structures in future studies toward topological superconductivity.

See the supplementary material for extended methods and additional data.

AUTHOR DECLARATIONS
Conflict of Interest
The authors have no conflicts to disclose.

Author Contributions
I.V., V.Z., and L.S. grew the InSb NF. S.S. fabricated the devices. S.S. and S.H. carried out the experiments. M.P.N. carried out the numerical simulations. S.S., M.C., and S.H. analyzed the data and wrote the manuscript with strong input from all coauthors.

DATA AVAILABILITY
The data that support the findings of this study are available from the corresponding author upon reasonable request.

REFERENCES
[1]F. D. M. Haldane, "Nobel Lecture: Topological quantum matter," Rev. Mod. Phys. **89**, 040502 (2017).

[2]C. Nayak, S. H. Simon, A. Stern, M. Freedman, and S. D. Sarma, "Non-Abelian anyons and topological quantum computation," Rev. Mod. Phys. **80**, 1083–1159 (2008).

[3]E. Prada, P. San-Jose, M. W. A. de Moor, A. Geresdi, E. J. H. Lee, J. Klinovaja, D. Loss, J. Nygård, R. Aguado, and L. P. Kouwenhoven, "From Andreev to Majorana bound states in hybrid superconductor-semiconductor nanowires," Nat. Rev. Phys. **2**, 575–594 (2020).

[4]A. Stern and N. H. Lindner, "Topological quantum computation—From basic concepts to first experiments," Science **339**, 1179–1184 (2013).

[5]A. Fornieri, A. M. Whiticar, F. Setiawan, E. Portolés, A. C. C. Drachmann, A. Keselman, S. Gronin, C. Thomas, T. Wang, R. Kallaher, G. C. Gardner, E. Berg, M. J. Manfra, A. Stern, C. M. Marcus, and F. Nichele, "Evidence of topological superconductivity in planar Josephson junctions," Nature **569**, 89–92 (2019).

[6]C. M. Moehle, C. T. Ke, Q. Wang, C. Thomas, D. Xiao, S. Karwal, M. Lodari, V. van de Kerkhof, R. Termaat, G. C. Gardner, G. Scappucci, M. J. Manfra, and S. Goswami, "InSbAs two-dimensional electron gases as a platform for topological superconductivity," arXiv:2105.10437 (2021).

[7]Y. Chen, S. Huang, J. Mu, D. Pan, J. Zhao, and H. Q. Xu, "A double quantum dot defined by top gates in a single crystalline InSb nanosheet," Chin. Phys. B (to be published, 2021).

[8]F. Qu, J. van Veen, F. K. de Vries, A. J. A. Beukman, M. Wimmer, W. Yi, A. A. Kiselev, B.-M. Nguyen, M. Sokolich, M. J. Manfra, F. Nichele, C. M. Marcus, and L. P. Kouwenhoven, "Quantized conductance and large g-factor anisotropy in InSb quantum point contacts," Nano Lett. **16**, 7509–7513 (2016).

[9]M. de la Mata, R. Leturcq, S. R. Plissard, C. Rolland, C. Magén, J. Arbiol, and P. Caroff, "Twin-induced InSb nanosails: A convenient high mobility quantum system," Nano Lett. **16**, 825–833 (2016).

[10]T. Ashley, A. B. Dean, C. T. Elliott, G. J. Pryce, A. D. Johnson, and H. Willis, "Uncooled high-speed InSb field-effect transistors," Appl. Phys. Lett. **66**, 481–483 (1995).

[11]R. J. Sladek, "Effective masses of electrons in indium arsenide and indium antimonide," Phys. Rev. **105**, 460–464 (1957).

[12]C. T. Ke, C. M. Moehle, F. K. de Vries, C. Thomas, S. Metti, C. R. Guinn, R. Kallaher, M. Lodari, G. Scappucci, T. Wang, R. E. Diaz, G. C. Gardner, M. J. Manfra, and S. Goswami, "Ballistic superconductivity and tunable π-junctions in InSb quantum wells," Nat. Commun. **10**, 3764 (2019).

[13]F. K. de Vries, M. L. Sol, S. Gazibegovic, R. L. M. o het Veld, S. C. Balk, D. Car, E. P. A. M. Bakkers, L. P. Kouwenhoven, and J. Shen, "Crossed Andreev reflection in InSb flake Josephson junctions," Phys. Rev. Res. **1**, 032031 (2019).

[14] Z. Lei, C. A. Lehner, E. Cheah, C. Mittag, M. Karalic, W. Wegscheider, K. Ensslin, and T. Ihn, "Gate-defined quantum point contact in an InSb two-dimensional electron gas," Phys. Rev. Res. **3**, 023042 (2021).

[15] I. Žutić, J. Fabian, and S. D. Sarma, "Spintronics: Fundamentals and applications," Rev. Mod. Phys. **76**, 323–410 (2004).

[16] V. Mourik, K. Zuo, S. M. Frolov, S. R. Plissard, E. P. A. M. Bakkers, and L. P. Kouwenhoven, "Signatures of Majorana fermions in hybrid superconductor-semiconductor nanowire devices," Science **336**, 1003–1007 (2012).

[17] H. A. Nilsson, P. Samuelsson, P. Caroff, and H. Q. Xu, "Supercurrent and multiple Andreev reflections in an InSb nanowire Josephson junction," Nano Lett. **12**, 228–233 (2012).

[18] S. Li, N. Kang, D. X. Fan, L. B. Wang, Y. Q. Huang, P. Caroff, and H. Q. Xu, "Coherent charge transport in ballistic InSb nanowire Josephson junctions," Sci. Rep. **6**, 24822 (2016).

[19] S. Gazibegovic, D. Car, H. Zhang, S. C. Balk, J. A. Logan, M. W. A. de Moor, M. C. Cassidy, R. Schmits, D. Xu, G. Wang, P. Krogstrup, R. L. M. O. het Veld, K. Zuo, Y. Vos, J. Shen, D. Bouman, B. Shojaei, D. Pennachio, J. S. Lee, P. J. van Veldhoven, S. Koelling, M. A. Verheijen, L. P. Kouwenhoven, C. J. Palmstrøm, and E. P. A. M. Bakkers, "Epitaxy of advanced nanowire quantum devices," Nature **548**, 434–438 (2017).

[20] O. Gül, H. Zhang, F. K. de Vries, J. van Veen, K. Zuo, V. Mourik, S. Conesa-Boj, M. P. Nowak, D. J. van Woerkom, M. Quintero-Pérez, M. C. Cassidy, A. Geresdi, S. Koelling, D. Car, S. R. Plissard, E. P. A. M. Bakkers, and L. P. Kouwenhoven, "Hard superconducting gap in InSb nanowires," Nano Lett. **17**, 2690–2696 (2017).

[21] O. Gül, H. Zhang, J. D. S. Bommer, M. W. A. de Moor, D. Car, S. R. Plissard, E. P. A. M. Bakkers, A. Geresdi, K. Watanabe, T. Taniguchi, and L. P. Kouwenhoven, "Ballistic Majorana nanowire devices," Nat. Nanotechnol. **13**, 192–197 (2018).

[22] S. T. Gill, J. Damasco, B. E. Janicek, M. S. Durkin, V. Humbert, S. Gazibegovic, D. Car, E. P. A. M. Bakkers, P. Y. Huang, and N. Mason, "Selective-area superconductor epitaxy to ballistic semiconductor nanowires," Nano Lett. **18**, 6121–6128 (2018).

[23] J. E. Sestoft, T. Kanne, A. N. Gejl, M. von Soosten, J. S. Yodh, D. Sherman, B. Tarasinski, M. Wimmer, E. Johnson, M. Deng, J. Nygård, T. S. Jespersen, C. M. Marcus, and P. Krogstrup, "Engineering hybrid epitaxial InAsSb/Al nanowires for stronger topological protection," Phys. Rev. Mater. **2**, 044202 (2018).

[24] M. Pendharkar, B. Zhang, H. Wu, A. Zarassi, P. Zhang, C. P. Dempsey, J. S. Lee, S. D. Harrington, G. Badawy, S. Gazibegovic, R. L. M. Op het Veld, M. Rossi, J. Jung, A.-H. Chen, M. A. Verheijen, M. Hocevar, E. P. A. M. Bakkers, C. J. Palmstrøm, and S. M. Frolov, "Parity-preserving and magnetic field–resilient superconductivity in InSb nanowires with Sn shells," Science **372**, 508–511 (2021).

[25] O. Lesser, A. Saydjari, M. Wesson, A. Yacoby, and Y. Oreg, "Phase-induced topological superconductivity in a planar heterostructure," Proc. Natl. Acad. Sci. U. S. A. **118**, e2107377118 (2021).

[26] D. Pan, D. X. Fan, N. Kang, J. H. Zhi, X. Z. Yu, H. Q. Xu, and J. H. Zhao, "Free-standing two-dimensional single-crystalline InSb nanosheets," Nano Lett. **16**, 834–841 (2016).

[27] J. Zhi, N. Kang, S. Li, D. Fan, F. Su, D. Pan, S. Zhao, J. Zhao, and H. Xu, "Supercurrent and multiple Andreev reflections in InSb nanosheet SNS junctions," Phys. Status Solidi B **256**, 1800538 (2019).

[28] J. Zhi, N. Kang, F. Su, D. Fan, S. Li, D. Pan, S. P. Zhao, J. Zhao, and H. Q. Xu, "Coexistence of induced superconductivity and quantum Hall states in InSb nanosheets," Phys. Rev. B **99**, 245302 (2019).

[29] I. Verma, V. Zannier, F. Rossi, D. Ercolani, F. Beltram, and L. Sorba, "Morphology control of single-crystal InSb nanostructures by tuning the growth parameters," Nanotechnology **31**, 384002 (2020).

[30] I. Verma, S. Salimian, V. Zannier, S. Heun, F. Rossi, D. Ercolani, F. Beltram, and L. Sorba, "High-mobility free-standing InSb nanoflags grown on InP nanowire stems for quantum devices," ACS Appl. Nano Mater. **4**, 5825–5833 (2021).

[31] N. Kang, D. Fan, J. Zhi, D. Pan, S. Li, C. Wang, J. Guo, J. Zhao, and H. Xu, "Two-dimensional quantum transport in free-standing InSb nanosheets," Nano Lett. **19**, 561–569 (2019).

[32] J. Xue, Y. Chen, D. Pan, J.-Y. Wang, J. Zhao, S. Huang, and H. Q. Xu, "Gate defined quantum dot realized in a single crystalline InSb nanosheet," Appl. Phys. Lett. **114**, 023108 (2019).

[33] Y. Chen, S. Huang, D. Pan, J. Xue, L. Zhang, J. Zhao, and H. Q. Xu, "Strong and tunable spin-orbit interaction in a single crystalline InSb nanosheet," npj 2D Mater. Appl. **5**, 3 (2021).

[34] S. Gazibegovic, G. Badawy, T. L. J. Buckers, P. Leubner, J. Shen, F. K. de Vries, S. Koelling, L. P. Kouwenhoven, M. A. Verheijen, and E. P. A. M. Bakkers, "Bottom-up grown 2D InSb nanostructures," Adv. Mater. **31**, 1808181 (2019).

[35] G. Grosso and G. P. Parravicini, *Solid State Physics* (Academic Press, 2000).

[36] F. Rohlfing, G. Tkachov, F. Otto, K. Richter, D. Weiss, G. Borghs, and C. Strunk, "Doppler shift in Andreev reflection from a moving superconducting condensate in Nb/InAs Josephson junctions," Phys. Rev. B **80**, 220507 (2009).

[37] M. Amado, A. Fornieri, F. Carillo, G. Biasiol, L. Sorba, V. Pellegrini, and F. Giazotto, "Electrostatic tailoring of magnetic interference in quantum point contact ballistic Josephson junctions," Phys. Rev. B **87**, 134506 (2013).

[38] H. Y. Günel, N. Borgwardt, I. E. Batov, H. Hardtdegen, K. Sladek, G. Panaitov, D. Grützmacher, and T. Schäpers, "Crossover from Josephson effect to single interface Andreev reflection in asymmetric superconductor/nanowire junctions," Nano Lett. **14**, 4977–4981 (2014).

[39] S. Guiducci, M. Carrega, F. Taddei, G. Biasiol, H. Courtois, F. Beltram, and S. Heun, "Full electrostatic control of quantum interference in an extended trenched Josephson junction," Phys. Rev. B **99**, 235419 (2019).

[40] S. Guiducci, M. Carrega, G. Biasiol, L. Sorba, F. Beltram, and S. Heun, "Toward quantum Hall effect in a Josephson junction," Phys. Status Solidi RRL **13**, 1800222 (2019).

[41] M. Carrega, S. Guiducci, A. Iorio, L. Bours, E. Strambini, G. Biasiol, M. Rocci, V. Zannier, L. Sorba, F. Beltram, S. Roddaro, F. Giazotto, and S. Heun, "Investigation of InAs-based devices for topological applications," Proc. SPIE **11090**, 110903Z (2019).

[42] G.-H. Lee and H.-J. Lee, "Proximity coupling in superconductor-graphene heterostructures," Rep. Prog. Phys. **81**, 056502 (2018).

[43] L. Banszerus, F. Libisch, A. Ceruti, S. Blien, K. Watanabe, T. Taniguchi, A. K. Hüttel, B. Beschoten, F. Hassler, and C. Stampfer, "Minigap and Andreev bound states in ballistic graphene," arXiv:2011.11471 (2021).

[44] J. K. Freericks, A. N. Tahvildar-Zadeh, and B. K. Nikolic, "Use of a generalized thouless energy in describing transport properties of Josephson junctions," IEEE Trans. Appl. Supercond. **15**, 896–899 (2005).

[45] K. K. Likharev, "Superconducting weak links," Rev. Mod. Phys. **51**, 101–159 (1979).

[46] J. P. Heida, B. J. van Wees, T. M. Klapwijk, and G. Borghs, "Nonlocal supercurrent in mesoscopic Josephson junctions," Phys. Rev. B **57**, R5618–R5621 (1998).

[47] N.-H. Kim, B.-K. Kim, H.-S. Kim, and Y.-J. Doh, "Fabrication and characterization of PbIn-Au-PbIn superconducting junctions," Prog. Supercond. Cryogenics **18**, 5–8 (2016).

[48] V. Barzykin and A. M. Zagoskin, "Coherent transport and nonlocality in mesoscopic SNS junctions: Anomalous magnetic interference patterns," Superlattices Microstruct. **25**, 797–807 (1999).

[49] D. E. Sheehy and A. M. Zagoskin, "Theory of anomalous magnetic interference pattern in mesoscopic superconducting/normal/superconducting Josephson junctions," Phys. Rev. B **68**, 144514 (2003).

[50] J. C. Cuevas, J. Hammer, J. Kopu, J. K. Viljas, and M. Eschrig, "Proximity effect and multiple Andreev reflections in diffusive superconductor–normal-metal–superconductor junctions," Phys. Rev. B **73**, 184505 (2006).

[51] J. C. Cuevas and F. S. Bergeret, "Magnetic interference patterns and vortices in diffusive SNS junctions," Phys. Rev. Lett. **99**, 217002 (2007).

[52] F. S. Bergeret and J. C. Cuevas, "The vortex state and Josephson critical current of a diffusive SNS junction," J. Low Temp. Phys. **153**, 304–324 (2008).

[53] F. Carillo, D. Born, V. Pellegrini, F. Tafuri, G. Biasiol, L. Sorba, and F. Beltram, "Relevant energy scale in hybrid mesoscopic Josephson junctions," Phys. Rev. B **78**, 052506 (2008).

[54] F. Chiodi, M. Ferrier, S. Guéron, J. C. Cuevas, G. Montambaux, F. Fortuna, A. Kasumov, and H. Bouchiat, "Geometry-related magnetic interference patterns in long SNS Josephson junctions," Phys. Rev. B **86**, 064510 (2012).

[55] T. D. Clark, R. J. Prance, and A. D. C. Grassie, "Feasibility of hybrid Josephson field effect transistors," J. Appl. Phys. **51**, 2736–2743 (1980).

[56] A. Chrestin, T. Matsuyama, and U. Merkt, "Critical currents and supercurrent oscillations in Josephson field-effect transistors," Phys. Rev. B **49**, 498–504 (1994).

[57]T. Akazaki, H. Takayanagi, J. Nitta, and T. Enoki, "A Josephson field effect transistor using an InAs-inserted-channel $In_{0.52}Al_{0.48}As/In_{0.53}Ga_{0.47}As$ inverted modulation-doped structure," Appl. Phys. Lett. **68**, 418–420 (1996).

[58]E. V. Bezuglyi, E. N. Bratus', and V. S. Shumeiko, "Resonant subgap current transport in Josephson field effect transistor," Phys. Rev. B **95**, 014522 (2017).

[59]F. Wen, J. Shabani, and E. Tutuc, "Josephson junction field-effect transistors for Boolean logic cryogenic applications," IEEE Trans. Electron Devices **66**, 5367–5374 (2019).

[60]G. E. Blonder, M. Tinkham, and T. M. Klapwijk, "Transition from metallic to tunneling regimes in superconducting microconstrictions: Excess current, charge imbalance, and supercurrent conversion," Phys. Rev. B **25**, 4515–4532 (1982).

[61]T. M. Klapwijk, G. E. Blonder, and M. Tinkham, "Explanation of subharmonic energy gap structure in superconducting contacts," Physica B **109–110**, 1657–1664 (1982).

[62]M. Octavio, M. Tinkham, G. E. Blonder, and T. M. Klapwijk, "Subharmonic energy-gap structure in superconducting constrictions," Phys. Rev. B **27**, 6739–6746 (1983).

[63]K. Flensberg, J. B. Hansen, and M. Octavio, "Subharmonic energy-gap structure in superconducting weak links," Phys. Rev. B **38**, 8707–8711 (1988).

[64]M. T. Deng, C. L. Yu, G. Y. Huang, M. Larsson, P. Caroff, and H. Q. Xu, "Anomalous zero-bias conductance peak in a Nb-InSb nanowire-Nb hybrid device," Nano Lett. **12**, 6414–6419 (2012).

[65]K. Gharavi, G. W. Holloway, R. R. LaPierre, and J. Baugh, "Nb/InAs nanowire proximity junctions from Josephson to quantum dot regimes," Nanotechnology **28**, 085202 (2017).

[66]M. Kjaergaard, H. J. Suominen, M. P. Nowak, A. R. Akhmerov, J. Shabani, C. J. Palmstrøm, F. Nichele, and C. M. Marcus, "Transparent semiconductor-superconductor interface and induced gap in an epitaxial heterostructure Josephson junction," Phys. Rev. Appl. **7**, 034029 (2017).

[67]A. Bardas and D. V. Averin, "Electron transport in mesoscopic disordered superconductor–normal-metal–superconductor junctions," Phys. Rev. B **56**, R8518–R8521 (1997).

[68]S. Heedt, M. Quintero-Pérez, F. Borsoi, A. Fursina, N. van Loo, G. P. Mazur, M. P. Nowak, M. Ammerlaan, K. Li, S. Korneychuk, J. Shen, M. A. Y. van de Poll, G. Badawy, S. Gazibegovic, N. de Jong, P. Aseev, K. van Hoogdalem, E. P. A. M. Bakkers, and L. P. Kouwenhoven, "Shadow-wall lithography of ballistic superconductor-semiconductor quantum devices," Nat. Commun. **12**, 4914 (2021).

[69]The next mode in the fit, the 41st mode, has $Tr = 0.15$ and, thus, does not contribute to the transport.

[70]A. M. Marsh, D. A. Williams, and H. Ahmed, "Supercurrent transport through a high-mobility two-dimensional electron gas," Phys. Rev. B **50**, 8118–8121 (1994).

[71]A. C. C. Drachmann, H. J. Suominen, M. Kjaergaard, B. Shojaei, C. J. Palmstrøm, C. M. Marcus, and F. Nichele, "Proximity effect transfer from NbTi into a semiconductor heterostructure via epitaxial aluminum," Nano Lett. **17**, 1200–1203 (2017).

[72]G. W. Webb, F. Marsiglio, and J. E. Hirsch, "Superconductivity in the elements, alloys and simple compounds," Physica C **514**, 17–27 (2015).

[73]J. Rumble, ed., *CRC Handbook of Chemistry and Physics*, 101st ed. (CRC Press, 2020).

[74]B. A. Aminov, A. A. Golubov, and M. Y. Kupriyanov, "Quasiparticle current in ballistic constrictions with finite transparencies of interfaces," Phys. Rev. B **53**, 365–373 (1996).

[75]C. Baumgartner, L. Fuchs, L. Frész, S. Reinhardt, S. Gronin, G. C. Gardner, M. J. Manfra, N. Paradiso, and C. Strunk, "Josephson inductance as a probe for highly ballistic semiconductor-superconductor weak links," Phys. Rev. Lett. **126**, 037001 (2021).

[76]M. Tinkham, *Introduction to Superconductivity* (McGraw-Hill, 1996).

[77]V. Ambegaokar and A. Baratoff, "Tunneling between superconductors," Phys. Rev. Lett. **10**, 486–489 (1963).

[78]I. O. Kulik and A. N. Omel'yanchuk, "Contribution to the microscopic theory of the Josephson effect in superconducting bridges," JETP Lett. **21**, 96–97 (1975); available at http://jetpletters.ru/ps/1463/article_22289.shtml

[79]C. W. J. Beenakker, "Universal limit of critical-current fluctuations in mesoscopic Josephson junctions," Phys. Rev. Lett. **67**, 3836–3839 (1991).

[80]W. Mayer, J. Yuan, K. S. Wickramasinghe, T. Nguyen, M. C. Dartiailh, and J. Shabani, "Superconducting proximity effect in epitaxial Al-InAs heterostructures," Appl. Phys. Lett. **114**, 103104 (2019).

[81]Y.-J. Doh, J. A. van Dam, A. L. Roest, E. P. A. M. Bakkers, L. P. Kouwenhoven, and S. D. Franceschi, "Tunable supercurrent through semiconductor nanowires," Science **309**, 272–275 (2005).

[82]J. Xiang, A. Vidan, M. Tinkham, R. M. Westervelt, and C. M. Lieber, "Ge/Si nanowire mesoscopic Josephson junctions," Nat. Nanotechnol. **1**, 208–213 (2006).

Supplementary Material

Gate-controlled Supercurrent in Ballistic InSb Nanoflag Josephson Junctions

Sedighe Salimian,[1] Matteo Carrega,[2] Isha Verma,[1] Valentina Zannier,[1] Michał P. Nowak,[3] Fabio Beltram,[1] Lucia Sorba,[1] and Stefan Heun[1, a)]

[1)] *NEST, Istituto Nanoscienze-CNR and Scuola Normale Superiore,*
Piazza San Silvestro 12, 56127 Pisa, Italy

[2)] *CNR-SPIN, Via Dodecaneso 33, 16146, Genova, Italy*

[3)] *AGH University of Science and Technology, Academic Centre for*
Materials and Nanotechnology, al. A. Mickiewicza 30, 30-059 Krakow,
Poland

(Dated: 18 November 2021)

[a)]stefan.heun@nano.cnr.it

I. EXTENDED METHODS

The InSb nanoflags were grown by chemical beam epitaxy (CBE) from metal-organic precursors in a Riber Compact-21 system. Initially, InP nanowires were grown on InP(111)B substrates via Au-assisted growth. The catalyst particles were 30 nm Au colloids drop-casted onto the bare substrate. The InP nanowire stems were grown with sample rotation for 90 minutes at 400°C, with 0.6 Torr TMIn (trimethylindium) and 1.2 Torr TBP (tert-butylphosphine). Then the growth temperature was reduced by 30°C (in presence of TBP flux only) to the InSb growth temperature. The InSb nanoflags were grown without rotation, after aligning the $\langle 112 \rangle$ crystal direction toward the Sb precursor beam, as described in Ref.[1], initially for 30 min with 0.6 Torr TMIn and 2.3 Torr TMSb (trimethylantimony), and then for additional 60 min, linearly increasing the TMSb line pressure from 2.3 to 2.6 Torr, in order to enhance the asymmetric radial growth.[1]

To fabricate the devices, the as-grown InSb NFs were dry transferred onto a prepatterned highly conductive p-type Si(111) substrate, which serves as a global back gate. A 285 nm thick SiO_2 layer covers the Si substrate as dielectric. During the mechanical transfer, the InSb NFs are detached from the InP NW stems, so that well-isolated InSb NFs were found lying randomly distributed on the substrate. The position of selected InSb NFs was determined relative to predefined alignment markers using SEM images. Considering the thickness and the edge geometry of the InSb NFs, electrodes were patterned on a 400 nm thick layer of AR-P 679.04 resist with standard electron-beam lithography (EBL). Prior to metal deposition, the native oxides were removed using a sulfur-based cleaning method which results also in a smoother InSb surface.[2] To this end, the native oxide was etched for 1 min in an optimized sulfur solution of $(NH_4)_2S_x$ (1:9 $(NH_4)_2S_x$:DI water at 40°C). Then the samples were rinsed in DI water for 30 s. Next, a 10/150 nm Ti/Nb film was deposited with high deposition rate after an intense pre-sputtering of each target, followed by lift off in hot acetone.

All devices in this work were measured in four-terminal configuration at 250 mK using a ^{3}He cryostat equipped with RC- and π-filters. Signals were registered via room-temperature preamplifiers. In most cases (Figs. 1,3,4,5 of the main paper), data were measured in DC + AC configuration, in which the DC setup allowed to measure $I - V$ curves, while a small AC component added to the DC bias allowed to measure the differential resistance with a

lock-in amplifier, with current excitation in the range $5 - 10$ nA. On the other hand, the data shown in Fig. 2 were measured just in DC, without the AC component. The differential resistance was in this case obtained by numerical differentiation. Except for Fig. 2 of the main paper, all measurements were performed at a small magnetic field of $B_0 = 6$ mT used to compensate for the residual magnetization of the cryostat.

For the analysis of the experimental conductance traces, we follow the approach of Ref.[3]. We calculate the total conductance G of a multimode Josephson junction as the sum of N_i single-mode contributions resulting from the transverse quantization, contained in M families, where modes in each family are characterized by their transmission probability Tr_i.[4] We obtain N_i, Tr_i, and the induced superconducting gap Δ^* by optimizing the numerically calculated conductance to the experimental one by a least squares fit. M is a free parameter of the fitting procedure and chosen as the smallest number for which at least one of the parameters Tr_i is zero.
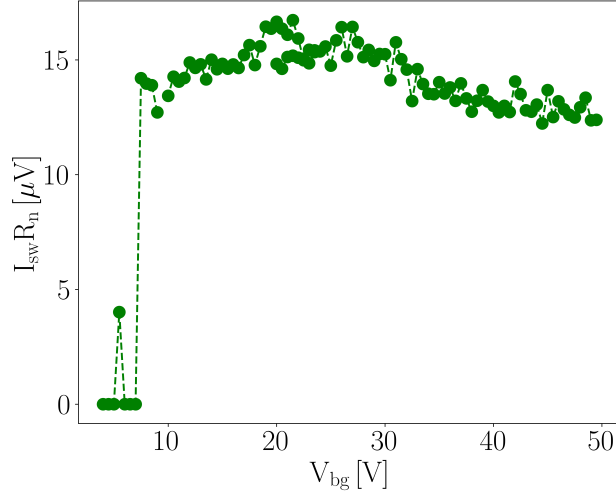
II. ADDITIONAL DATA

FIG. S1. Switching current I_{sw} times normal resistance R_n versus back gate voltage V_{bg}, obtained by analysis from the data shown in Fig. 3 of the main text. The product $I_{sw} \cdot R_n$ remains nearly constant at 15 μV for a wide range of back gate voltages. Device SC10 G4 1-5.
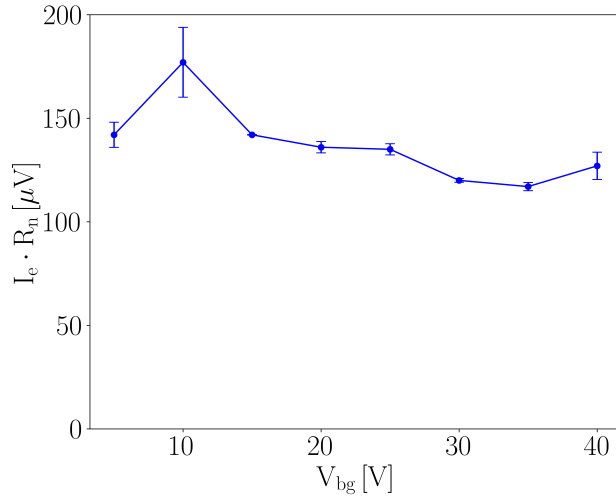

FIG. S2. Excess current I_e times normal resistance R_n versus back gate voltage V_{bg}. Error bars are the standard deviation of the measured data. The product $I_e \cdot R_n$ remains nearly constant at (137 ± 19) μV for a wide range of back gate voltages. Device SC10 G4 1-5.

All data shown in the main paper were measured from the same device, SC10 G4 1-5. We have measured other devices and obtained consistent results. Below we show results from devices SC10 G5 3-2A and SC20 F7 5-2.
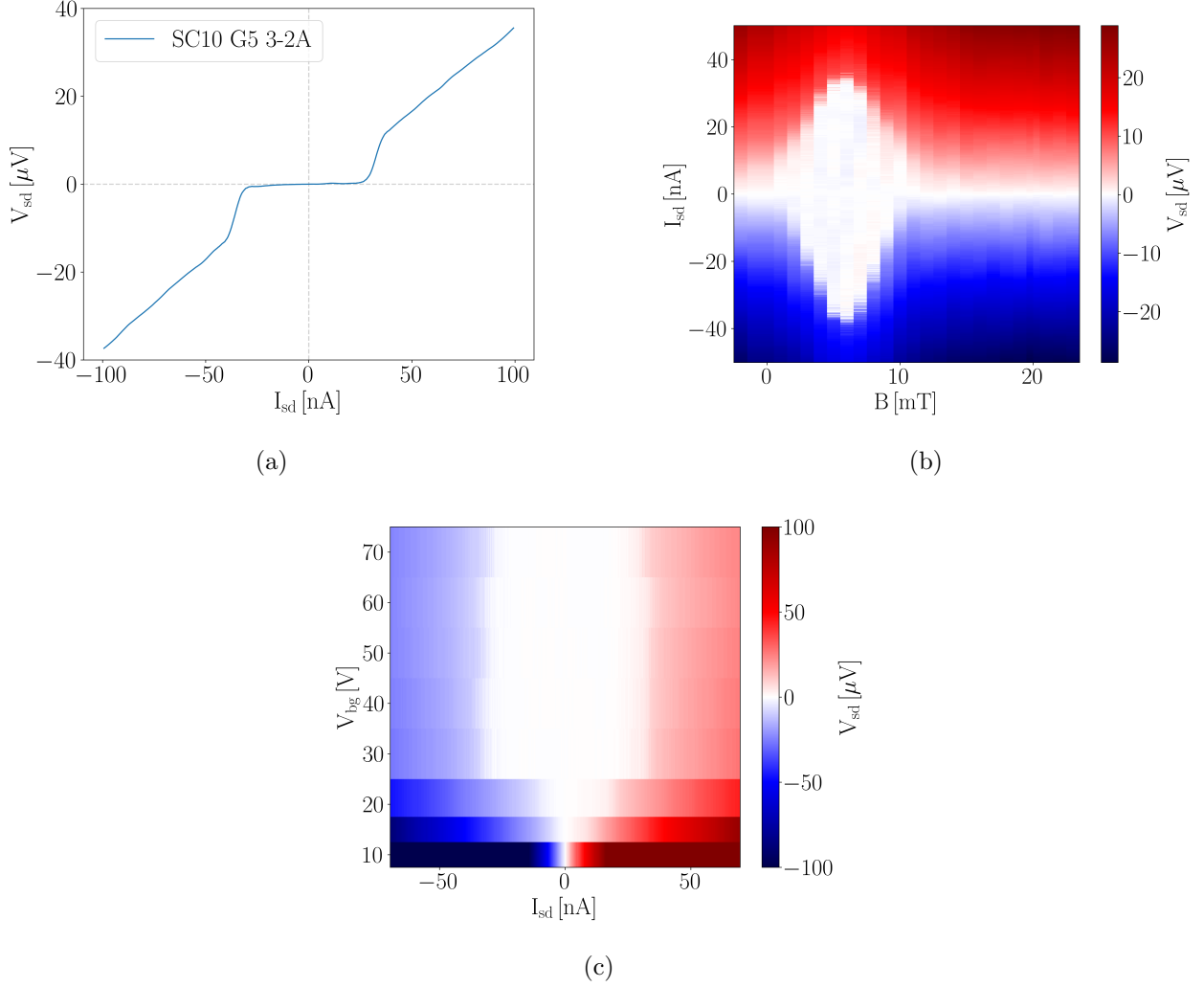

(a)

(b)

(c)

FIG. S3. **Device SC10 G5 3-2A.** (a) Voltage drop V_{sd} as a function of bias current I_{sd}. A supercurrent of ~ 30 nA is observed. $V_{bg} = 40$ V, $T = 250$ mK, $B = 5$ mT. (b) 2D colormap of voltage drop V_{sd}, plotted vs. current bias I_{sd} and magnetic field B, measured at $V_{bg} = 40$ V and $T = 250$ mK. (c) Color-scale plot of voltage drop V_{sd} as a function of current bias I_{sd} and back gate voltage V_{bg}. $T = 250$ mK. $B = 6$ mT.
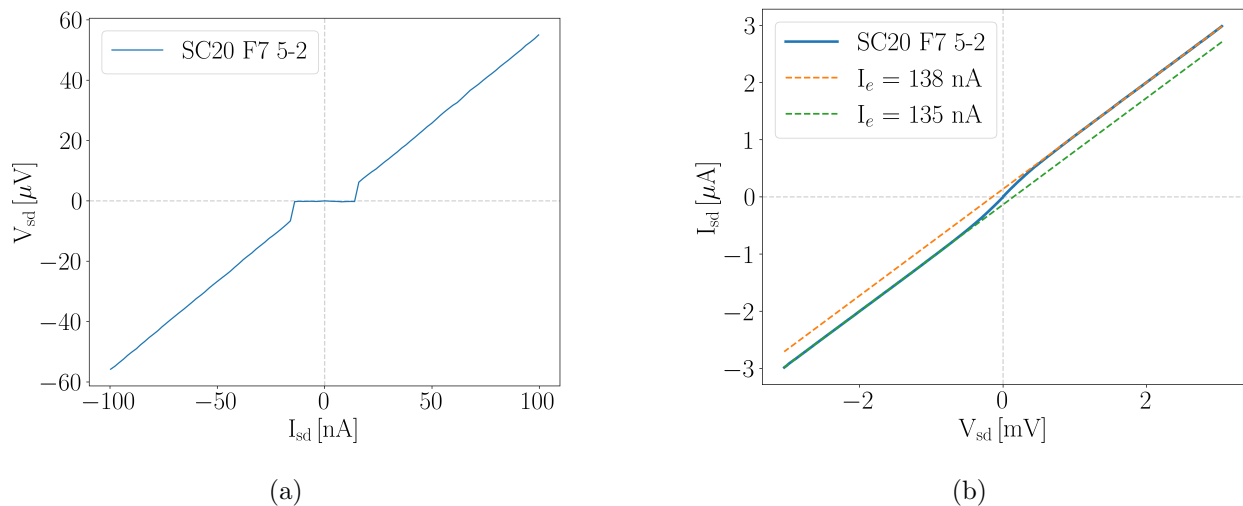
FIG. S4. **Device SC20 F7 5-2.** (a) Voltage drop V_{sd} as a function of bias current I_{sd}. A supercurrent of ~ 15 nA is observed. $V_{bg} = 20$ V, $T = 250$ mK, $B = 15$ mT. (b) $I-V$ characteristics measured in DC. The linear fit (dashed lines) of the $I-V$ curve for $V_{sd} > \pm 2$ mV gives the excess current I_e as the intercept at zero bias voltage. The normal resistance R_n is 1072 Ω. This gives a product $I_e \cdot R_n = 147$ μV, in good agreement with the value obtained from device SC10 G4 1-5. $T = 250$ mK and $V_{bg} = 40$ V. $B = 14$ mT applied to compensate for the residual magnetization of the cryostat.

REFERENCES

[1] I. Verma, S. Salimian, V. Zannier, S. Heun, F. Rossi, D. Ercolani, F. Beltram, and L. Sorba, "High-Mobility Free-Standing InSb Nanoflags Grown on InP Nanowire Stems for Quantum Devices," ACS Appl. Nano Mater. **4**, 5825–5833 (2021).

[2] O. Gül, H. Zhang, F. K. de Vries, J. van Veen, K. Zuo, V. Mourik, S. Conesa-Boj, M. P. Nowak, D. J. van Woerkom, M. Quintero-Pérez, M. C. Cassidy, A. Geresdi, S. Koelling, D. Car, S. R. Plissard, E. P. A. M. Bakkers, and L. P. Kouwenhoven, "Hard Superconducting Gap in InSb Nanowires," Nano Lett. **17**, 2690–2696 (2017).

[3] D. Averin and A. Bardas, "ac Josephson Effect in a Single Quantum Channel," Phys. Rev. Lett. **75**, 1831–1834 (1995).

[4] A. Bardas and D. V. Averin, "Electron transport in mesoscopic disordered superconductor–normal-metal–superconductor junctions," Phys. Rev. B **56**, R8518–R8521 (1997).